JOURNAL OF THE AMERICAN COLLEGE OF CARDIOLOGY
© 2014 BY THE AMERICAN COLLEGE OF CARDIOLOGY FOUNDATION
PUBLISHED BY ELSEVIER INC.
VOL. 64, NO. 22, 2014
ISSN 0735-1097/$36.00
http://dx.doi.org/10.1016/j.jacc.2014.09.029

OCT Assessment of the Long-Term Vascular Healing Response 5 Years After Everolimus-Eluting Bioresorbable Vascular Scaffold

Antonios Karanasos, MD,* Cihan Simsek, MD,* Muthukarrupan Gnanadesigan, MSc,†
Nienke S. van Ditzhuijzen, MSc,* Raphael Freire, MD,* Jouke Dijkstra, PhD,‡ Shengxian Tu, PhD,‡
Nicolas Van Mieghem, MD,* Gijs van Soest, PhD,† Peter de Jaegere, MD, PhD,* Patrick W. Serruys, MD, PhD,*
Felix Zijlstra, MD, PhD,* Robert-Jan van Geuns, MD, PhD,* Evelyn Regar, MD, PhD*

ABSTRACT

BACKGROUND Although recent observations suggest a favorable initial healing process of the everolimus-eluting bioresorbable vascular scaffold (BVS), little is known regarding long-term healing response.

OBJECTIVES This study assessed the in vivo vascular healing response using optical coherence tomography (OCT) 5 years after elective first-in-man BVS implantation.

METHODS Of the 14 living patients enrolled in the Thoraxcenter Rotterdam cohort of the ABSORB A study, 8 patients underwent invasive follow-up, including OCT, 5 years after implantation. Advanced OCT image analysis included luminal morphometry, assessment of the adluminal signal-rich layer separating the lumen from other plaque components, visual and quantitative tissue characterization, and assessment of side-branch ostia "jailed" at baseline.

RESULTS In all patients, BVS struts were integrated in the vessel and were not discernible. Both minimum and mean luminal area increased from 2 to 5 years, whereas lumen eccentricity decreased over time. In most patients, plaques were covered by a signal-rich, low-attenuating layer. Minimum cap thickness over necrotic core was 155 ± 90 μm. One patient showed plaque progression and discontinuity of this layer. Side-branch ostia were preserved with tissue bridge thinning that had developed in the place of side-branch struts, creating a neo-carina.

CONCLUSIONS At long-term BVS follow-up, we observed a favorable tissue response, with late luminal enlargement, side-branch patency, and development of a signal-rich, low-attenuating tissue layer that covered thrombogenic plaque components. The small size of the study and the observation of a different tissue response in 1 patient warrant judicious interpretation of our results and confirmation in larger studies. (J Am Coll Cardiol 2014;64:2343–56) © 2014 by the American College of Cardiology Foundation.

Metallic stents for percutaneous revascularization have been associated with late complications, such as neoatherosclerosis, late restenosis, and thrombosis (1). Bioresorbable vascular scaffolds (BVS) could help overcome such pitfalls. In the ABSORB A study (ABSORB [A bioabsorbable everolimus-eluting coronary stent system] Clinical Investigation, Cohort A), the first-generation

From the *Department of Interventional Cardiology, Thoraxcenter, Erasmus University Medical Center, Rotterdam, the Netherlands; †Department of Biomedical Engineering, Thoraxcenter, Erasmus University Medical Center, Rotterdam, the Netherlands; and the ‡Division of Image Processing, Department of Radiology, Leiden University Medical Center, Leiden, the Netherlands. The Thoraxcenter receives unrestricted grants from Abbott and St. Jude Medical. Dr. Karanasos has received funding support from Hellenic Heart Foundation and St. Jude Medical. Dr. Simsek and Mr. Gnanadesigan were supported by research grants from "Nederlandse Hartstichting" (2009B091 to Dr. Simsek and 2010B064 to Mr. Gnanadesigan). Dr. Tu is employed by Medis Medical Imaging Systems; and has a research appointment at the Leiden University Medical Center. Dr. van Geuns has received speaker fees and research grants from Abbott Vascular. All other authors have reported that they have no relationships relevant to the contents of this paper to disclose.
Listen to this manuscript's audio summary by *JACC* Editor-in-Chief Dr. Valentin Fuster.
You can also listen to this issue's audio summary by *JACC* Editor-in-Chief Dr. Valentin Fuster.

Manuscript received March 7, 2014; revised manuscript received August 28, 2014, accepted September 5, 2014.

ABBREVIATIONS AND ACRONYMS

BVS = bioresorbable vascular scaffold(s)

ICC = intraclass correlation coefficient

IQR = interquartile range

IVUS = intravascular ultrasound

OCT = optical coherence tomography

SB = side branch

everolimus-eluting BVS (Absorb BVS 1.0; Abbott Vascular, Santa Clara, California) was associated with a good long-term clinical outcome after 2 and 5 years (2,3). Plaque regression from 2 to 5 years and recovery of vasomotion in the scaffolded segment were documented in a patient subset (4). Moreover, recent clinical observations of a signal-rich layer separating potentially thrombogenic plaque components from the lumen (5,6) suggest a favorable long-term healing response with potential plaque sealing.

SEE PAGE 2357

We aimed to provide a comprehensive optical coherence tomography (OCT) analysis of the vascular healing response in the longest follow-up available to date (5 years) in the first series of patients who received everolimus-eluting BVS.

METHODS

PATIENT POPULATION. The study population (4) and index procedure (2) have been described (Online Appendix). Briefly, all 14 living patients from the Thoraxcenter Rotterdam cohort of ABSORB A were asked to participate. Eight consented and were included. The protocol was approved by the institutional ethics committee and conformed to the Declaration of Helsinki.

OCT IMAGE ACQUISITION. All 8 subjects underwent frequency-domain OCT at the 5-year invasive follow-up (7). Six patients at baseline, 7 patients at 6-month follow-up, and 7 patients at 2-year follow-up had undergone occlusive time-domain OCT per the study protocol, with serial OCT imaging at all intervals available for 5 patients. For details, see the Online Appendix.

DEFINITIONS. OCT analysis of bioresorbable scaffolds reveals essential differences from metal stents (**Figure 1**). With metal stents, struts are preserved and neointimal area is clearly defined as the area between stent and lumen contour. In BVS, when scaffold struts are still discernible, the neointimal area can be assessed similarly to metal stents. However, at long-term follow-up, BVS scaffold struts are no longer visible, and the area corresponding to struts and neointima has similar optical properties as the underlying fibrous layer (5,8). Consequently, it is impossible to distinguish between strut area, neointimal area, and underlying plaque.

Therefore, the vascular structure observed at the scaffolded segment, a product of the consolidation of underlying plaque, biodegraded struts, and neointima, resembled a native atherosclerotic plaque and was defined as neoplaque (**Figure 1**).

Because OCT cannot distinguish the scaffold area, and thus neointimal area, from the underlying plaque, neointimal thickness cannot be assessed directly. Hence, we aimed to provide an indirect assessment that focused on the signal-rich layer, which consisted of the neointimal layer, resorbed struts, and preexisting fibrous tissue. We analyzed this signal-rich layer, between the lumen border and internal elastic lamina, for providing a measure of separation of the lumen from underlying plaque components (5,6). In situations in which signal-poor regions (e.g., calcifications, necrotic core, deeply located fibrous plaque) obscured delineation of the internal elastic lamina, the signal-rich layer was delineated between lumen border and the boundary of signal-rich and signal-poor regions (**Figures 1 and 2**).

OCT IMAGE ANALYSIS. The platinum scaffold markers defined the region of interest. Quantitative and qualitative 5-year OCT image analysis was performed per frame. Analysis included the assessment of discernible struts, lumen morphometry, signal-rich layer thickness measurement, neoplaque characterization, attenuation analysis, and ostial side-branch (SB) assessment. Metal stents implanted in the same vessels were also analyzed (1).

LUMINAL MEASUREMENTS AND VARIABILITY ANALYSIS. For details, see the Online Appendix. Measurements included mean and minimum lumen area and eccentricity, calculated as: ratio (maximum lumen diameter – minimum lumen diameter)/maximum lumen diameter (7). Lumen measurements were assessed for intraobserver, interobserver, and intrastudy variability.

QUANTIFICATION OF SIGNAL-RICH LAYER THICKNESS. The signal-rich layer was quantified following segmentation of its luminal and abluminal contour by measuring minimum, mean, and maximum thickness and symmetry (ratio of minimal to maximal thickness) (**Figure 2**). Signal-rich layer measurements were assessed for variability.

NEOPLAQUE CHARACTERIZATION. Neoplaque morphology was assessed per frame at 5 years, according to native atherosclerosis definitions (7), and the arc of calcifications, necrotic core, and mixed plaque were measured with QCU-CMS (LKEB, Leiden University, the Netherlands; research version of QIvus, Medis medical imaging systems, Leiden, the Netherlands). Fibrous cap contours were traced over necrotic core with mean and minimum cap thickness calculated per patient. Spread-out maps representing neoplaque morphology and cap thickness

throughout the scaffolded segment were generated (Figure 3) and color-coded by plaque type. The presence of sharply delineated signal-poor voids, which corresponded to intimal microchannels (7), was recorded. In neoplaques with necrotic core, OCT images were compared with previous follow-ups to look for de novo accumulation of necrotic core of adluminal origin, possibly corresponding to neoatherosclerosis.

ATTENUATION ANALYSIS. We used attenuation analysis for quantitative tissue characterization of the signal-rich layer and the neoplaque (Figure 4). In ex vivo validation experiments, highly attenuating regions (attenuation coefficient $\mu_t \geq 8$ mm^{-1}) have been associated with necrotic core or macrophages. Conversely, $\mu_t < 6$ mm^{-1} were associated with healthy vessel, intimal thickening, or calcified plaque (9,10). Attenuation was quantified circumferentially at different depths from the lumen surface by custom-made software (11). Results were plotted in spread-out maps demonstrating: 1) maximum attenuation coefficient per A-line throughout the pullback; and 2) attenuation coefficient values in different depths from the vessel surface.

SB ASSESSMENT. To assess anatomic SB jailing over time, 3-dimensional images of SB ostia were obtained by volume-rendering software (INTAGE Realia, KGT, Tokyo, Japan) (12). No struts were identifiable by OCT, but neointimal bridges had developed in their place and were classified based on their relative location to the ostium as proximal, distal, proximal and distal, or crossing (Figure 5). Mean and minimal thickness was measured in matched frames at 2- and 5-year follow-up with QCU-CMS (Online Figure 1).

SB ostium area was assessed with dedicated software (QAngioOCT 1.0, Medis Specials, Leiden, the Netherlands). After 3-dimensional reconstruction, a cut-plane perpendicular to the SB centerline was selected and SB ostium planimetry performed (Figure 6) (13).

STATISTICAL ANALYSIS. Continuous variables are presented as mean ± SD or median (interquartile range [IQR]) and nominal variables as n (%). Significance level was set at $p < 0.05$. Luminal measurements were compared by Wilcoxon signed-rank test. All other paired comparisons were performed by paired Student *t* test. No corrections were made for multiple comparisons. Variability was assessed with intraclass correlation coefficients (ICCs) for absolute agreement and Bland-Altman statistics. Statistical analysis was performed with SPSS version 20.0 (IBM, Armonk, New York).

FIGURE 1 Long-Term Vascular Healing Response in Metal Stents and Bioresorbable Scaffolds

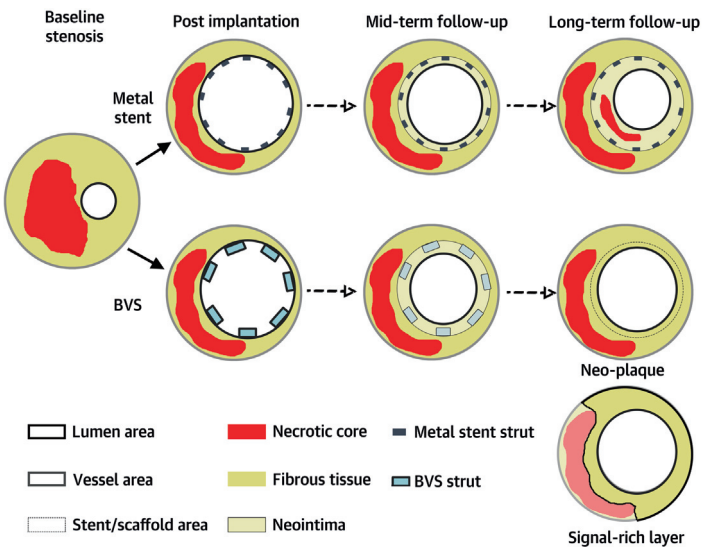

After metal stent implantation, struts are preserved and the neointimal area clearly delineated between stent and lumen contour even at long-term follow-up, with possible development of neoatherosclerosis within the neointima. Conversely, in long-term follow-up of bioresorbable scaffolds, neointimal boundaries are unclear after bioresorption **(dotted line)**, and the intima resembles native plaque, defined as *neoplaque*. The signal-rich layer is the layer that separates the underlying plaque components from the lumen. BVS = bioresorbable vascular scaffold.

RESULTS

LUMEN AND STRUT MEASUREMENTS. No binary restenosis was witnessed in the 5-year angiograms. In all patients, scaffold struts were no longer discernible as a result of complete bioresorption, and lumen area increased significantly from 2 to 5 years (Figure 7). Lumen eccentricity declined over time (baseline 0.24 ± 0.13; 6-month follow-up 0.29 ± 0.12; 2-year follow-up 0.21 ± 0.08; 5-year follow-up 0.15 ± 0.02; $p < 0.05$ for all comparisons vs. previous studies).

The total strut count was reduced in 5 patients with serial observations: 278 struts at baseline, 248 at 6 months, 174 at 2 years, and no visible struts at 5 years. Two cases with incomplete scaffold apposition at baseline or 6 months demonstrated complete resolution of incomplete scaffold apposition at 2 years and complete strut bioresorption at 5 years.

QUANTIFICATION OF SIGNAL-RICH LAYER. Median values (IQR) for mean, minimum, and maximum signal-rich layer thickness and symmetry were 330 μm (290 to 378 μm), 150 μm (120 to 190 μm), 570 μm (500 to 640 μm), and 0.26 (0.20 to 0.33), respectively.

FIGURE 2 Quantifying Signal-Rich Layer Thickness in Different Plaque Types

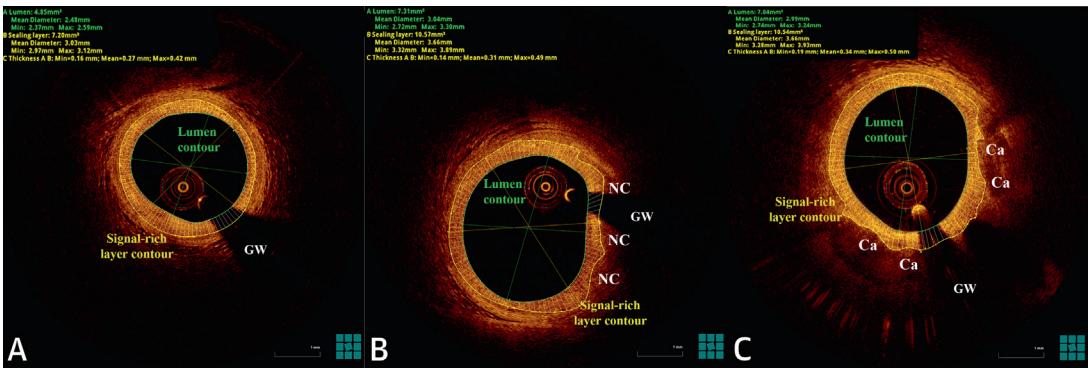

In the absence of attenuating intimal regions, the contour is traced at the internal elastic lamina **(A)**. In plaques with necrotic core, the abluminal contour is traced at the attenuating region boundary **(B)**. In plaques with calcifications, the signal-rich layer is segmented at the calcification edge **(C)**. Ca = calcium; GW = guidewire; NC = necrotic core.

FIGURE 3 Plaque Characterization and Cap Tracing

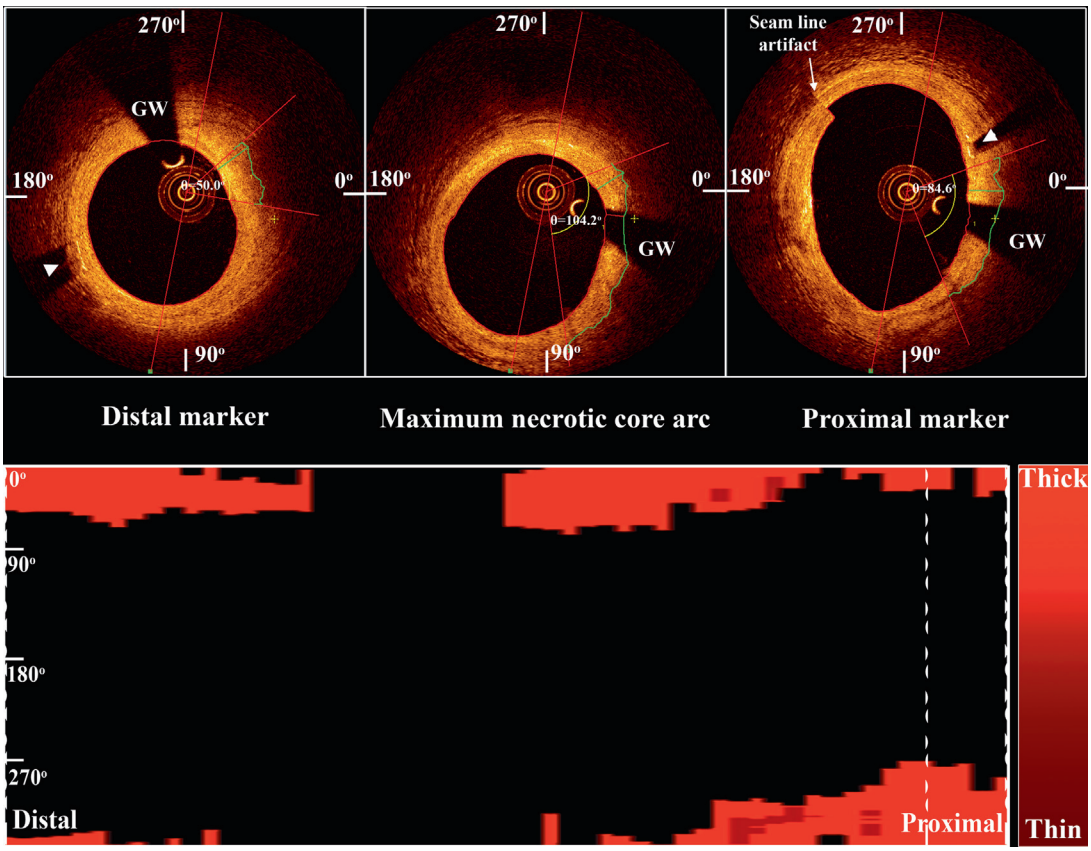

In frames with necrotic core, calcifications, or mixed plaque within the scaffolded segment, the overlying fibrous cap was segmented and minimum thicknesses were recorded. A spread-out map was generated that showed the component distribution within the neoplaque, with lighter colors corresponding to thicker caps. **Arrowhead** indicates scaffold marker. GW = guidewire.

FIGURE 4 Example of Attenuation Analysis

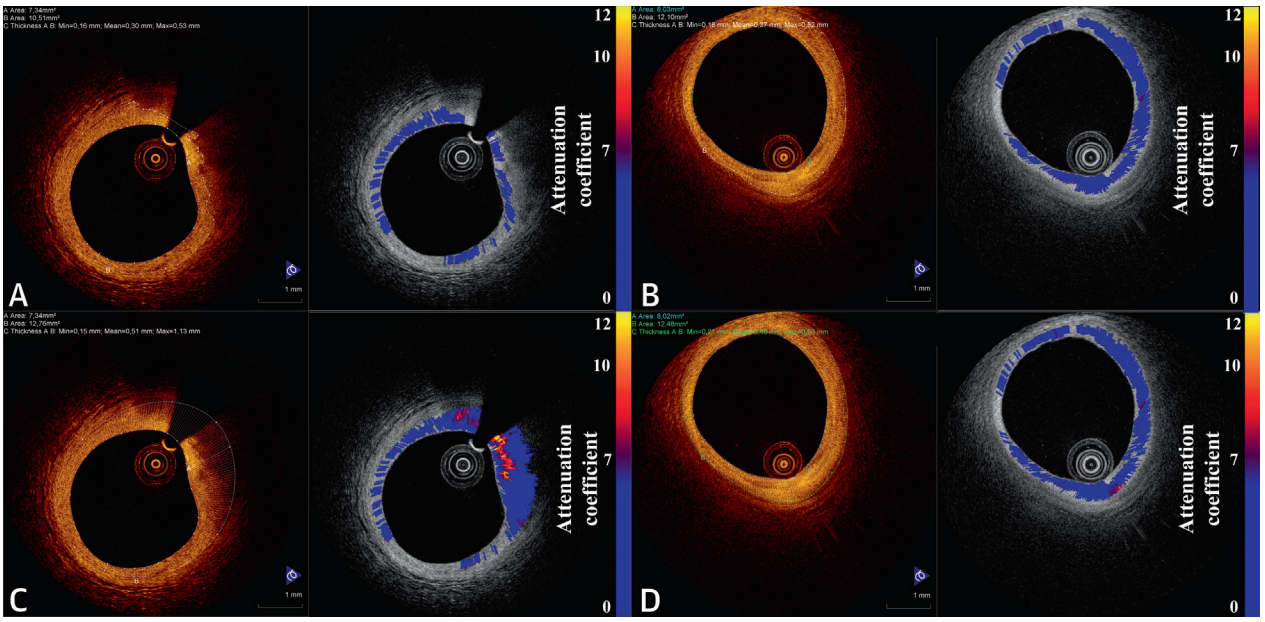

In all frames, tissue attenuation properties within adluminal and abluminal contour were measured and displayed on a color scale (**blue** represents low-attenuation regions, whereas **red** and **yellow** represent high-attenuation regions). Analysis was performed in the signal-rich layer **(A, B)**, as defined in Figure 2, and in the entire neoplaque, up to the internal elastic lamina **(C, D)**. Note the lack of highly attenuating regions within the signal-rich layer **(A, B)**, whereas attenuation properties deeper in the neoplaque depended on tissue type (high attenuation in necrotic core; **C**). For intimal thickness $<$200 μm, as in 6 to 7 o'clock in **A** and **C** and 8 to 9 o'clock in **B** and **D**, analysis was not performed because of lack of a sufficient imaging window. Abbreviations as in Figure 2.

FIGURE 5 Different Types of Tissue Bridges Overlying Side Branches

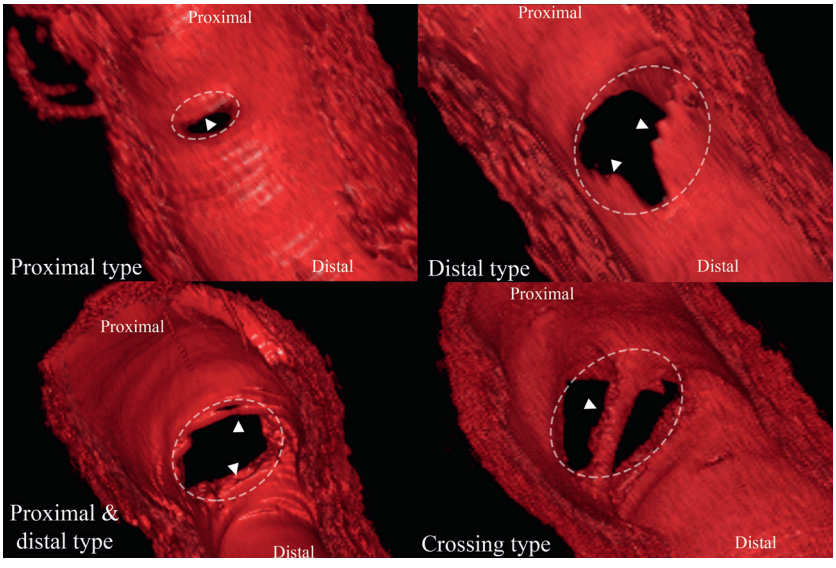

Classification was based on the relative location with the side-branch ostium. Four different types could be identified: proximal, distal, proximal and distal, or crossing. **Dotted lines** indicate side-branch ostia; **arrowhead** indicates tissue bridge.

FIGURE 6 Side-Branch Ostium Area Measurement by Cut-Plane Analysis

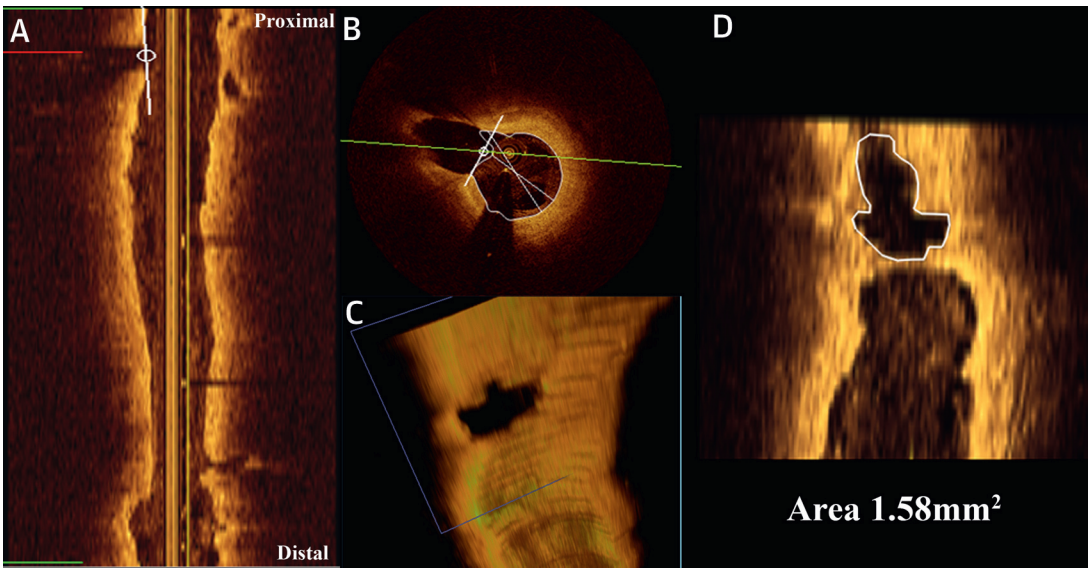

After 3-dimensional rendering, side-branch ostium area could be measured in a cut plane perpendicular to the side-branch ostium: L-mode display **(A)**; cross-sectional image **(B)**; 3-dimensional rendering **(C)**; derived perpendicular cut plane **(D)**.

Online Figure 2 demonstrates frequency distributions of these thickness measurements.

NEOPLAQUE CHARACTERIZATION. Figure 8 presents spread-out neoplaque maps. The mean value of minimum cap thickness was 310 ± 113 μm, whereas the minimum value was 155 ± 90 μm. Mean and maximum values were 92° ± 49° and 156° ± 72° for necrotic core arc, 80° and 104° for calcification arc, and 104° ± 145° and 146° ± 80° for mixed-plaque arc.

Microchannels were identified in 7 of 8 patients and in 66 of 468 frames (14.1%). Per the neoplaque maps, necrotic core or mixed plaque >1 quadrant was observed in 7 patients. Comparison with previous follow-ups did not reveal evidence of de novo necrotic core accumulation of adluminal origin.

Two patients had a focally irregular lumen contour. Patient #8 had a short intimal dissection, not present at earlier investigations, at the overlap between BVS and a metallic stent implanted at baseline. This minor, angiographically not visible dissection was most likely iatrogenic, induced by the guidewire. In Patient #4, a thin-cap fibroatheroma was observed at the distal scaffold segment with cap disruption and small thrombus (Figure 9). Post-hoc revision of previous OCT examinations revealed possible scaffold discontinuity near the distal edge at 4 months, with the scaffold being dislocated opposite to the rupture site.

ATTENUATION ANALYSIS. Mean per-patient attenuation within the signal-rich layer was 1.77 ± 0.32 mm^{-1}, and the median was 1.28 ± 0.25 mm^{-1} (Online Figure 3). This value was higher within the entire neoplaque (mean per patient 2.87 ± 0.54 mm^{-1}; median per patient 2.33 ± 0.49 mm^{-1}; $p < 0.001$) (Online Figure 4). Spread-out attenuation maps at different depths from the luminal surface are displayed in Figure 10. The surface layers (first 200 μm) had low attenuation, overlying high-attenuation areas located deeper in the plaque.

SB ASSESSMENT. All SBs were patent with TIMI (Thrombolysis In Myocardial Infarction) flow grade 3. Overall, 14 SBs were associated with incompletely apposed struts at previous examinations. Neointimal bridges at 5 years were identified in 13 SBs, whereas in 1, no bridge was visible (Table 1).

Minimal and mean thickness of neointimal bridges overlying SBs were respectively reduced from 241 ± 92 μm and 341 ± 106 μm at 2 years to 161 ± 107 μm and 227 ± 119 μm at 5 years ($p < 0.001$) (Online Figure 5).

METAL DRUG-ELUTING STENT ANALYSIS. Metal drug-eluting stent (DES) analysis is presented in Online Table 1 and Figure 11. In all metal stents, coverage was >95%, without malapposed struts, whereas neoatherosclerosis was identified in all.

VARIABILITY ANALYSIS. Interobserver and intraobserver variability for both frame- and patient-level analysis was low (interobserver: difference 0.23 ± 0.29 mm, ICC = 0.98; interobserver [core laboratory]: difference 0.13 ± 0.32 mm, ICC = 0.98; intraobserver: difference 0.17 ± 0.19 mm, ICC = 0.99) (Online Table 2, Online Figure 6). As seen in the Bland-Altman plots, there were few measurements with significant differences, all of which were in the polygon of confluence of larger SBs with complex geometry lacking a priori definitions for contour tracing. ICCs for mean and minimal signal-rich layer thickness were respectively 0.95 and 0.86 for intraobserver variability and 0.80 and 0.80 for interobserver variability.

DISCUSSION

We present the first in vivo long-term OCT data after BVS implantation. Despite the small sample size, these first patients treated with BVS offer a unique opportunity to study the long-term vascular response after BVS implantation (**Figure 12**). Our main findings are that 5 years after BVS 1.0 implantation: 1) there is late lumen enlargement with simultaneous increase in luminal symmetry; 2) all struts have disappeared and have been integrated within the neointima and underlying plaque, forming a homogeneous, signal-rich, low-attenuating layer; 3) this signal-rich layer separates the lumen from the underlying plaque with a minimum thickness of 150 μm (IQR: 120 to 190 μm); 4) this effect is not universal, with 1 case showing thinning and disruption of the signal-rich layer; 5) jailed SB ostia are preserved, whereas SB-related struts have been replaced by thin tissue bridges; and 6) metal DES in the same vessels are lacking a distinct signal-rich layer and show neoatherosclerosis despite good coverage and apposition (**Central Illustration**).

In our series, we observed a consistent luminal enlargement from 2 to 5 years in all patients. Late luminal enlargement in bioresorbable scaffolds has been attributed to outward remodeling in animal studies (14) and plaque burden reduction in clinical trials (4,15). Our findings echo larger-scale intravascular ultrasound (IVUS) observations of lumen area increases from 6 months to 2 years after BVS implantation (2,15). IVUS observations in our study population were consistent with our findings, displaying a trend for further lumen enlargement from 2 to 5 years, driven by a persistent decrease in plaque size from 6 months to 2 years caused by either true plaque regression or pseudoregression from strut resorption (2,4). A similar trend was observed in the 5-year multislice computed tomography follow-up of ABSORB A (3). We observed recovery of luminal symmetry, a finding of unclear significance. Simultaneous observations of strut bioresorption and signal-rich layer development suggest a potentially favorable biological effect, which parallels IVUS studies showing increased plaque rupture in eccentric vessels (16). The observed complete strut bioresorption tracks with vasomotion findings demonstrating a lack of mechanical vessel constraint, with positive acetylcholine response in 4 patients, negative response in 2 patients, and absence of significant change in 2 patients (4).

FIGURE 7 Serial Luminal Measurements

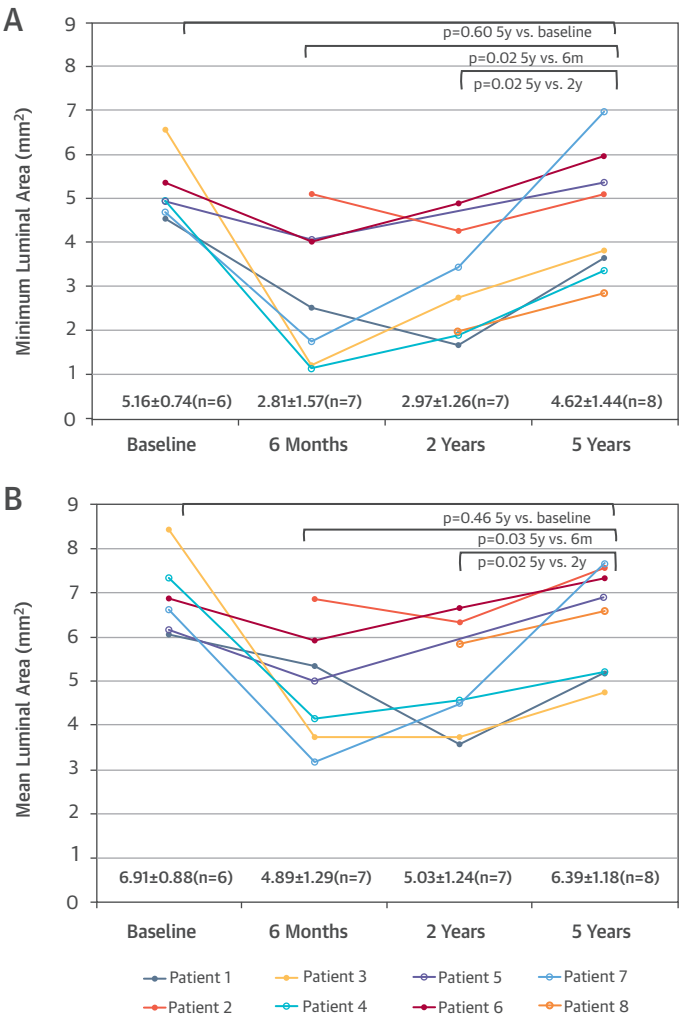

Despite an initial decrease in lumen dimensions from baseline to 6 months, minimal **(A)** and mean **(B)** lumen areas were increased at 5 years compared with previous follow-ups and were not significantly different from baseline.

FIGURE 8 Neoplaque Morphology

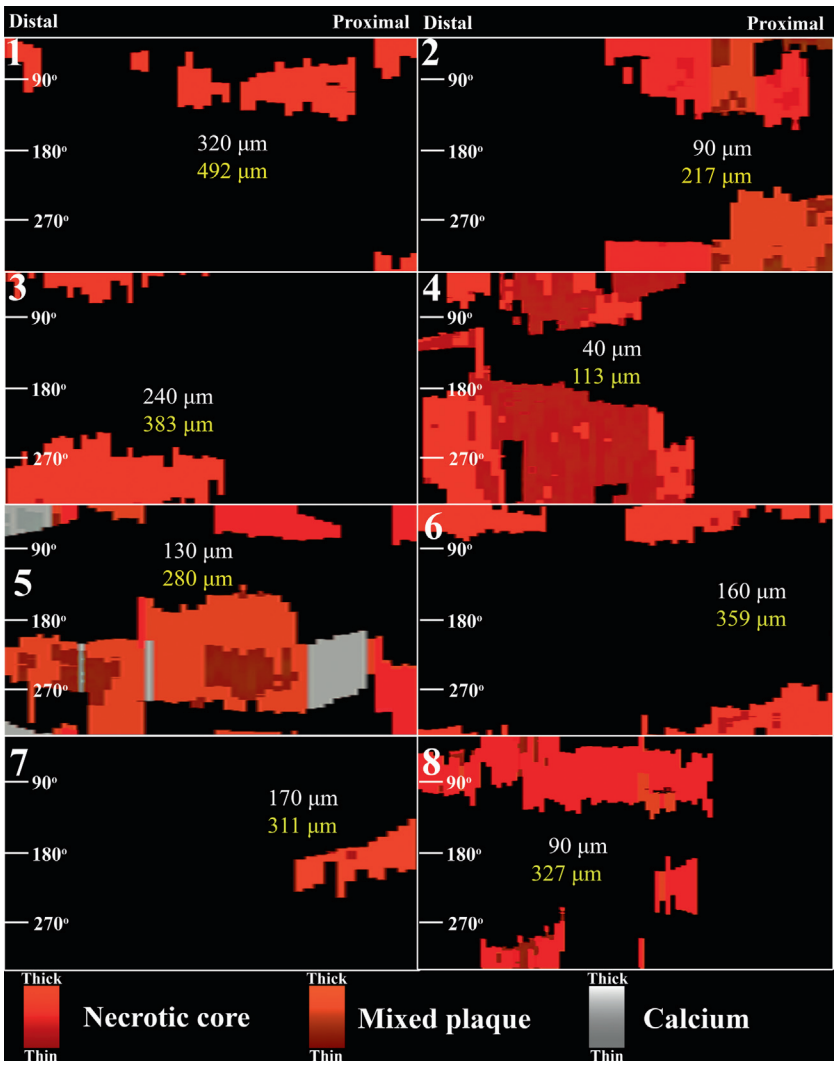

Spread-out maps from all patients demonstrating neoplaque composition. **Red** represents necrotic core; **orange**, mixed plaque; and **white**, calcification. **Lighter colors** indicate a thicker fibrous cap (>250 μm). The minimum and mean values of minimum cap thickness per patient are presented in **white** and **yellow**, respectively.

It has been suggested that neointimal growth after BVS resorption could serve as a mechanical barrier that prevents potentially thrombogenic plaque components from reaching the bloodstream, a concept dubbed "plaque sealing" or "recapping the plaque" (5,6). With this hypothesis in mind, we scrutinized BVS morphology in our cohort, using sophisticated algorithms for in-depth analysis. We focused on the developed adluminal signal-rich layer, which corresponds to neointima, bioresorbed struts, and fibrous components of the underlying plaque. The minimum signal-rich layer thickness was 150 μm, and the minimum cap thickness over necrotic core was 155 ± 90 μm, both well beyond the 65-μm threshold generally accepted as high risk for plaque rupture (17), which suggests that this layer could reliably separate the lumen from potentially thrombogenic plaque components. Importantly, this layer showed remarkable homogeneity in the attenuation analysis, with low attenuation values hinting at the absence of high-risk wall components such as necrotic core and macrophages (9,10). This signal-rich layer could be protective against very late scaffold thrombosis or de novo thrombosis by plaque progression and rupture (1,17).

The complete scaffold integration into the vascular wall has shaped a neoplaque phenotype that resulted from the complex interaction of pre-existing plaque, morphological changes of the pre-existing plaque subject to dynamic local rheological factors (18,19), strut resorption, and neointima formation (8). We visually characterized neoplaque using standardized OCT criteria (7). Quantitative attenuation analysis corroborated these qualitative findings, revealing colocalization of necrotic core regions with high attenuation regions (Online Figure 7), generally located deeper in the vessel wall and rarely observed within the first 200 μm from luminal surface. Of note, most patients were receiving intensive medical therapy (statins, 75%; beta-blockers, 75%; angiotensin receptor blockers, 62.5%), which possibly contributed to this favorable phenotype.

Metal stents covered with well-organized and functional neointima can likewise present a mechanical barrier between underlying plaque and lumen. However, neointimal proliferation and neoatherosclerosis development over time have been reported for bare-metal stents and are even more accelerated for DES. The permanent nature of the metallic structure further limits the vessel's capacity for remodeling, plaque regression, and lumen enlargement over time. Consequently, lumen narrowing develops inevitably over time, and indeed, 3 metal DES in our cohort showed adluminal neoatherosclerosis, with minimum cap thickness ranging from 70 to 110 μm. This is notable because thin fibrous cap emerges as a risk factor for neointimal rupture and acute coronary syndrome not only in native atherosclerosis but also in neoatherosclerosis (1).

We analyzed the fate of SBs "jailed" by BVS, because high strut thickness and tissue bridge formation have raised questions regarding long-term patency (12). Three-dimensional rendering demonstrated SB patency, allowed reliable ostial measurements, and identified different intimal bridge patterns. Strut integration into these tissue bridges was completed, accompanied by bridge thinning from 341 ± 106 μm at 2 years to 227 ± 119 μm at 5 years. Together with the angiographically confirmed absence of flow impairment, we consider these findings a favorable long-term outcome. However, the implications of BVS over large SBs or in true bifurcation lesions remain unknown (20,21), because these were excluded per protocol.

Overall, our long-term OCT observations suggest a favorable vascular healing response with late lumen enlargement, increased luminal symmetry, SB patency, complete strut resorption, and formation of a potentially protective tissue layer, giving an appearance consistent with the hypothetical concept of plaque sealing. Patient #4 did show a different response, which captured our attention. We observed target-lesion progression, with OCT findings consistent with macrophage infiltration, abluminal necrotic core accumulation, fibrous cap thinning, and plaque rupture at follow-up, while the patient was treated only with aspirin and clopidogrel. This patient had diffuse disease that necessitated non-target-lesion revascularization with a metal

FIGURE 9 Vascular Response in Patient #4

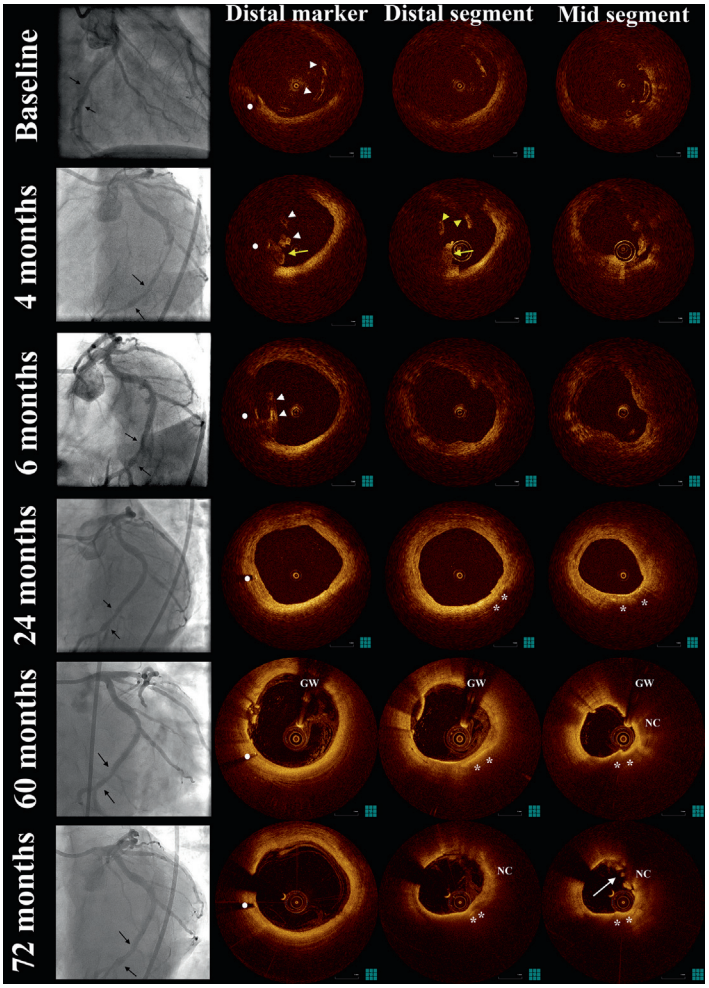

At baseline, there was malapposition **(white arrowheads)** at the distal segment. At 106-day follow-up, scaffold collapse **(white arrowheads)** at the site of the distal marker **(white bullet)**, overhanging struts **(yellow arrowheads)**, and thrombus **(yellow arrow)** were observed that suggested late scaffold discontinuity. At 6 months, a tissue bridge was formed **(white arrowheads)** at the site of the collapsed scaffold and integrated into the vascular wall by 24 months. Note the macrophage accumulation **(white asterisks)** at the opposite side at 24 months. At 60-month follow-up, lesion progression with macrophages and necrotic core was evident, as well as intimal disruption. At 72-month follow-up, there was further luminal narrowing and plaque rupture with thrombus **(white arrow)**. **Black arrows** indicate scaffold markers. Abbreviations as in Figure 2.

FIGURE 10 Attenuation Spread-Out Maps

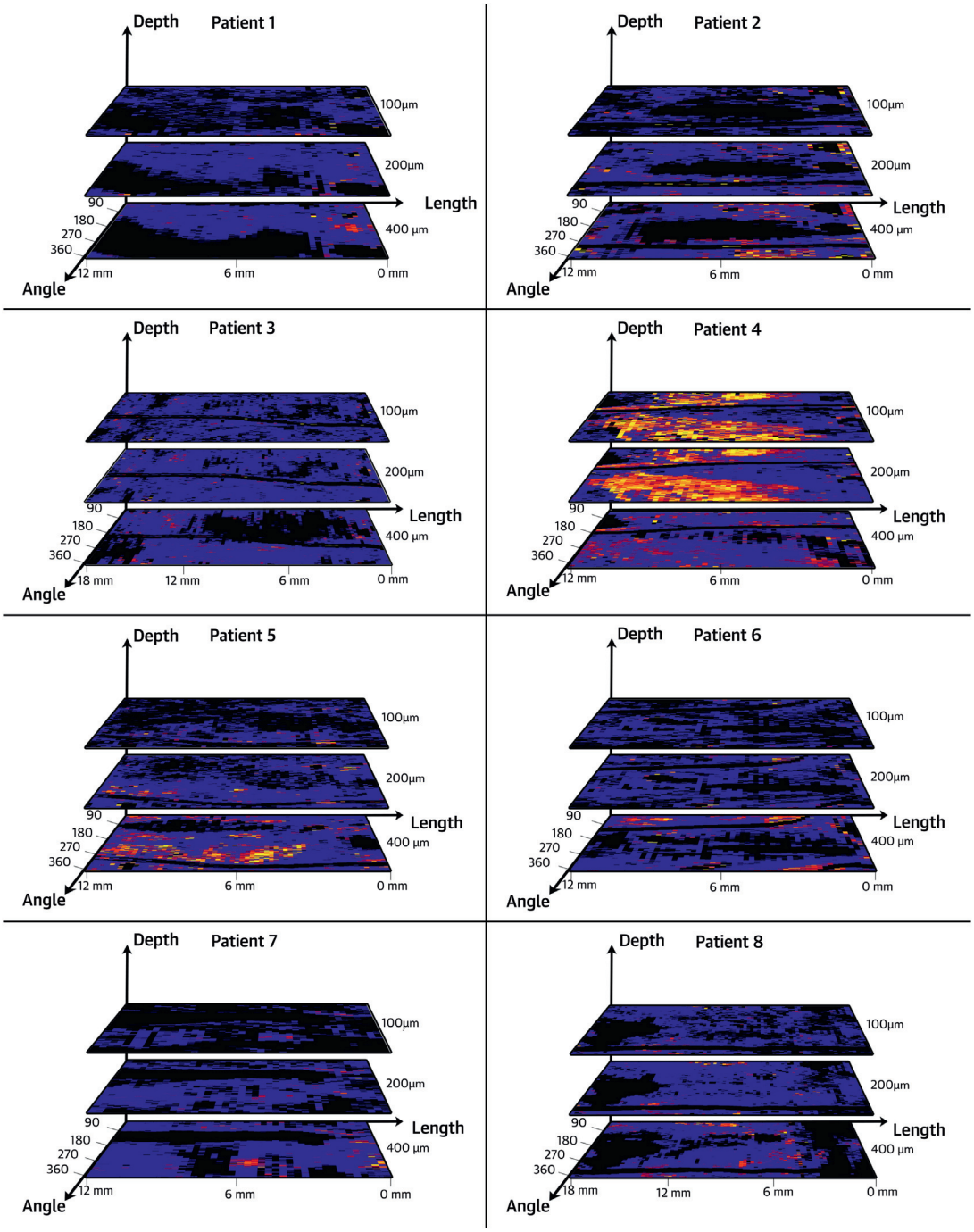

Spread-out maps demonstrating attenuation coefficient in pre-defined depths from the vessel surface (100, 200, and 400 μm) per patient. In most patients, there was a low-attenuating layer of 200 μm separating the underlying plaque (starting at ~400 μm) from the lumen. In Patient #4, this layer was absent, and attenuating areas were close to the lumen.

TABLE 1 Side-Branch Analysis

	Bifurcation Type	SB Ostium Area (mm²)	Jailing Pattern
Patient #1: SB 1	OM-LCx	4.81	Proximal and distal
Patient #2: SB 1	LAD-septal	6.22	Crossing
Patient #2: SB 2	LAD-diagonal	1.14	Distal
Patient #2: SB 3	LAD-septal	1.89	Proximal
Patient #3: SB 1	LAD-diagonal	1.58	Distal
Patient #3: SB 2	LAD-septal	1.42	N/A*
Patient #4: SB 1	LCx-OM	1.11	Proximal and distal
Patient #5: SB 1	LAD-septal	1.93	Crossing
Patient #5: SB 2	LAD-diagonal	0.46	Distal
Patient #6: SB 1	LCx-OM	1.37	Crossing
Patient #6: SB 2	OM-LCx	2.23	Distal
Patient #8: SB 1	LCx-OM	N/A†	Proximal
Patient #8: SB 2	LCx-posterolateral	0.3	Proximal
Patient #8: SB 3	LCx-OM	0.78	Proximal

*The bridge was not present at 5 years; distal location at previous studies. †Exact area not measurable.

LAD = left anterior descending coronary artery; LCx = left circumflex coronary artery; N/A = not available; OM = obtuse marginal branch; SB = side branch.

paclitaxel-eluting stent in the same artery 106 days after BVS implantation. This stent developed subsequent neoatherosclerosis with neointimal disruption and microthrombus formation (Figure 11). This evidence of accelerated atherosclerosis, combined with mechanical factors (baseline incomplete scaffold apposition followed by late structural discontinuity), might have contributed to the adverse neoplaque phenotype. Notably, the patient did not have a clinically apparent acute coronary syndrome regardless of these impressive findings.

Despite the limited scale of our study, it provides crucial information on the long-term vascular response 5 years after BVS implantation. Although we consider the overall vascular response to be favorable and in line with larger-scale clinical reports, there might be lessons to learn from observations in the single patient who showed a different biological reaction, with recurring plaque rupture after BVS implantation. This finding might underscore the need

FIGURE 11 Representative Optical Coherence Tomography Images of Metal Drug-Eluting Stents

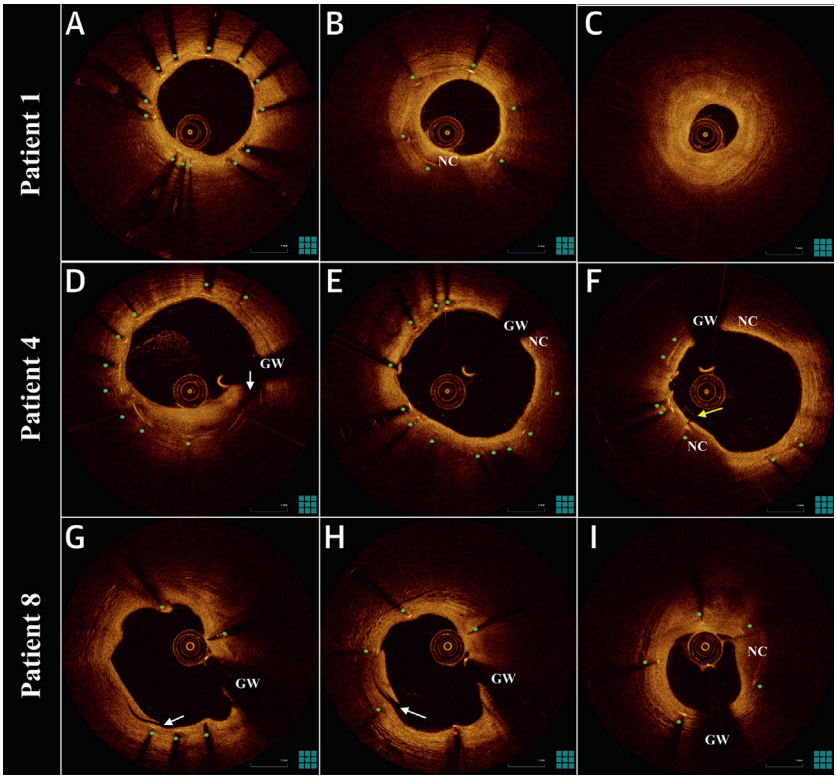

Covered struts **(A, green bullet)**; neoatherosclerosis **(B)**; distal edge stenosis **(C)** (area = 1.74 mm²); heterogeneous neointima with discontinuity **(D, white arrow)**; neoatherosclerosis **(E)**; neointimal disruption **(yellow arrow)** over necrotic core with mural micro-thrombi **(F)**; evaginations-neointimal discontinuity **(white arrow)** possibly iatrogenic **(G)**; uncovered strut **(H, red bullet)**; neoatherosclerosis **(I)**. Abbreviations as in Figure 2.

FIGURE 12 Serial Assessment of Vascular Response

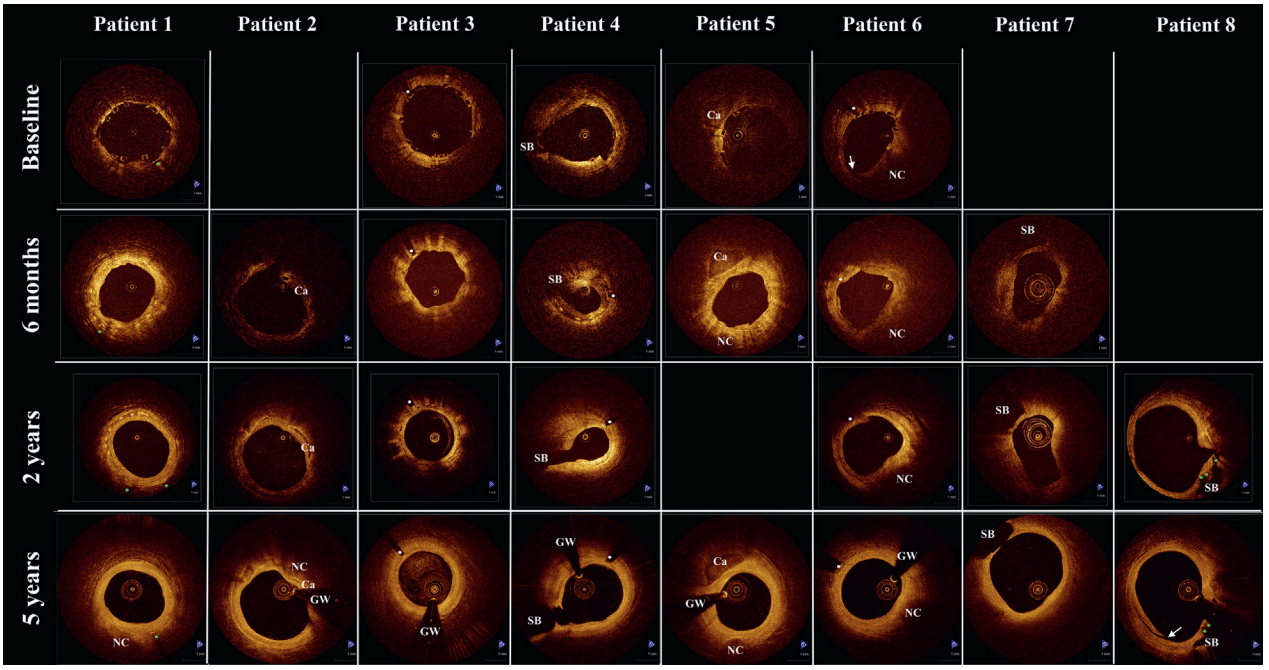

Matched representative images from serial examinations of all patients. Note the complete strut integration at 5 years, together with lumen enlargement, compared with 6-month and 2-year follow-ups. In Patient #8, intimal discontinuity **(arrow)**, presumably iatrogenic, was observed. **Green bullets** indicate metal struts; **white bullets** indicate scaffold markers. SB = side branch; other abbreviations as in Figure 2.

CENTRAL ILLUSTRATION Long-term Vascular Healing in Bioresorbable Scaffolds

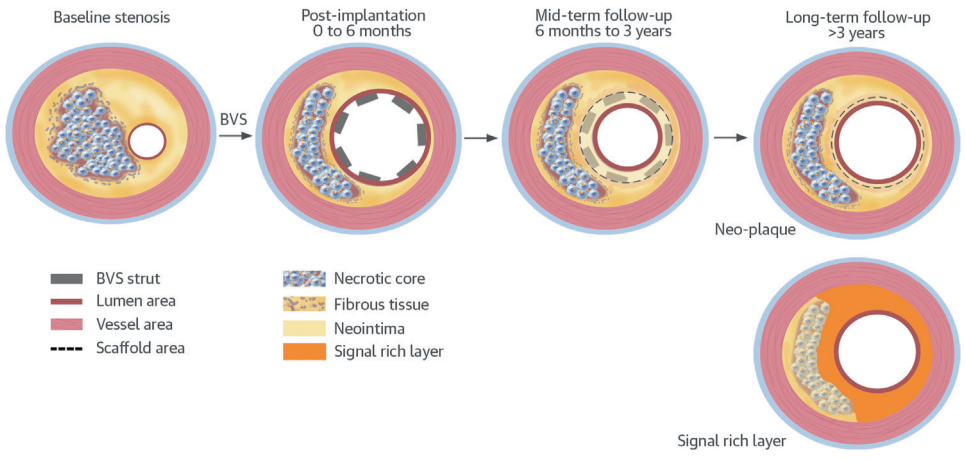

Karanasos, A. et al. J Am Coll Cardiol. 2014; 64(22):2343–56.

At long-term follow-up, bioresorbable vascular scaffolds (BVS) disappear, leaving behind late luminal enlargement, side-branch patency, and a signal-rich, low-attenuating tissue layer that covers the thrombogenic plaque components.

for an optimal acute mechanical result with optimal lesion coverage, while simultaneously raising questions regarding a possible responder/nonresponder reaction to BVS and the need for intensified secondary prevention in selected patients (22). As such, our findings might guide further research for optimizing the clinical efficacy of BVS in light of the 1.1 version modifications and herald observations in more complex populations (23).

STUDY LIMITATIONS. This is a small first-in-man study, so selection bias cannot be excluded, although the baseline clinical and angiographic characteristics were not different from the entire ABSORB A cohort. The BVS 1.0 assessed in our study differs in geometry and resorption rate from the currently used BVS 1.1, which might affect the temporal course and pattern of the healing response.

Attenuation analysis has only been validated in ex vivo specimens of native atherosclerosis and not in device-induced tissue responses. However, because attenuation is an optical property of tissue components, we expect the absence of high-attenuating regions to correspond to absence of necrotic core or macrophages in this setting.

Five-year OCT follow-up was performed with a nonocclusive frequency-domain system; previous OCT examinations were performed with an occlusive time-domain system. Frequency-domain OCT offers better image quality and higher dynamic range, which allows superior visualization of deeply located plaques (24). Because of these limitations of time-domain systems, serial assessment of plaque morphology was not performed systematically and was only examined with reference to possible neoatherosclerosis, although changes over time would be expected (19). Occlusive time-domain OCT slightly underestimates lumen area (25). Nevertheless, 4 patients in our study underwent additional nonocclusive OCT imaging at 2-year follow-up. When we compared nonocclusive data at 2 and 5 years, findings of late lumen enlargement were consistent, albeit not reaching significance because of the smaller sample size (minimum lumen area 3.54 ± 1.43 mm^2 at 2 years vs. 4.06 ± 1.33 mm^2 at 5 years; $p = 0.14$; mean lumen area 5.12 ± 1.62 mm^2 at 2 years vs. 5.95 ± 1.20 mm^2 at 5 years; $p = 0.07$).

CONCLUSIONS

At long-term follow-up 5 years after BVS implantation, we observed a favorable tissue response with late luminal enlargement, complete strut bioresorption, and development of a low-attenuating, signal-rich layer that covered the underlying potentially thrombogenic plaque components. The small scale of our study and the observation of a different tissue response in 1 patient warrant judicious interpretation of our results and further confirmation in larger studies.

ACKNOWLEDGMENTS The authors would like to thank Dr. George Sianos for his role in the ABSORB A trial, Prof. Johan Reiber and Joan Tuinenburg of ClinFact Core-Lab for the external validation of the 5-year measurements, and Prof. Guillermo Tearney for his expert review of neoplaque morphology.

REPRINT REQUESTS AND CORRESPONDENCE: Dr. Evelyn Regar, Erasmus University Medical Center, Department of Cardiology, Thoraxcenter, BA-585, Gravendijkwal 230, 3015 CE Rotterdam, the Netherlands. E-mail: e.regar@erasmusmc.nl.

PERSPECTIVES

COMPETENCY IN MEDICAL KNOWLEDGE: Strut resorption and vascular healing after bioresorbable vascular scaffold implantation are associated with late lumen enlargement, increased lumen symmetry, side-branch patency, and formation of a potentially protective tissue layer over the long term.

COMPETENCY IN PATIENT CARE: Occasional observations of unfavorable healing response after bioresorbable scaffold implantation suggest a need for both optimum lesion coverage and continued secondary prevention strategies after deployment of bioresorbable vascular scaffolds.

TRANSLATIONAL OUTLOOK: Additional long-term follow-up studies are needed to more completely characterize the patterns of biodegradation associated with favorable and unfavorable changes in plaque morphology and clinical outcomes after implantation of bioresorbable vascular scaffolds.

REFERENCES

1. Karanasos A, Ligthart J, Witberg K, et al. Association of neointimal morphology by optical coherence tomography with rupture of neoatherosclerotic plaque very late after coronary stent implantation. Proc. SPIE 8565, Photonic Therapeutics and Diagnostics IX, 856542 (March 8, 2013). http://dx.doi.org/10.1117/12.2006331.

2. Serruys PW, Ormiston JA, Onuma Y, et al. A bioabsorbable everolimus-eluting coronary stent system (ABSORB): 2-year outcomes and results from multiple imaging methods. Lancet 2009;373:897–910.

3. Onuma Y, Dudek D, Thuesen L, et al. Five-year clinical and functional multislice computed tomography angiographic results after coronary implantation of the fully resorbable polymeric everolimus-eluting scaffold in patients with de novo coronary artery disease: the ABSORB cohort A trial. J Am Coll Cardiol Intv 2013;6:999–1009.

4. Simsek C, Karanasos A, Magro M, et al. Long-term invasive follow-up of the everolimus-eluting bioresorbable vascular scaffold: five-year results

of multiple invasive imaging modalities. EuroIntervention 2014 Oct 28 [E-pub ahead of print].

5. Karanasos A, Simsek C, Serruys P, et al. Five-year optical coherence tomography follow-up of an everolimus-eluting bioresorbable vascular scaffold changing the paradigm of coronary stenting? Circulation 2012;126:e89–91.

6. Brugaletta S, Radu MD, Garcia-Garcia HM, et al. Circumferential evaluation of the neointima by optical coherence tomography after ABSORB bioresorbable vascular scaffold implantation: can the scaffold cap the plaque? Atherosclerosis 2012;221:106–12.

7. Tearney GJ, Regar E, Akasaka T, et al. consensus standards for acquisition, measurement, and reporting of intravascular optical coherence tomography studies: a report from the International Working Group for Intravascular Optical Coherence Tomography Standardization and Validation [published correction appears in J Am Coll Cardiol 2012;59:1662]. J Am Coll Cardiol 2012;59:1058–72.

8. Onuma Y, Serruys PW, Perkins LE, et al. Intracoronary optical coherence tomography and histology at 1 month and 2, 3, and 4 years after implantation of everolimus-eluting bioresorbable vascular scaffolds in a porcine coronary artery model: an attempt to decipher the human optical coherence tomography images in the ABSORB trial. Circulation 2010;122:2288–300.

9. van Soest G, Goderie T, Regar E, et al. Atherosclerotic tissue characterization in vivo by optical coherence tomography attenuation imaging. J Biomed Opt 2010;15:011105.

10. Ughi GJ, Adriaenssens T, Sinnaeve P, Desmet W, D'Hooge J. Automated tissue characterization of in vivo atherosclerotic plaques by intravascular optical coherence tomography images. Biomed Opt Express 2013;4:1014–30.

11. Gnanadesigan M, van Soest G, White S, et al. Effect of temperature and fixation on the optical properties of atherosclerotic tissue: a validation study of an ex-vivo whole heart cadaveric model. Biomed Opt Express 2014;5:1038–49.

12. Okamura T, Onuma Y, García-García HM, et al. 3-Dimensional optical coherence tomography assessment of jailed side branches by bioresorbable vascular scaffolds: a proposal for classification. J Am Coll Cardiol Intv 2010;3:836–44.

13. Karanasos A, Tu S, van Ditzhuijzen NS, et al. A novel method to assess coronary artery bifurcations by OCT: cut-plane analysis for side-branch ostial assessment from a main vessel pullback. Eur Heart J Cardiovasc Imaging 2014 Sep 16 [E-pub ahead of print].

14. Strandberg E, Zeltinger J, Schulz DG, Kaluza GL. Late positive remodeling and late lumen gain contribute to vascular restoration by a non-drug eluting bioresorbable scaffold: a four-year intravascular ultrasound study in normal porcine coronary arteries. Circulation Cardiovasc Interv 2012;5:39–46.

15. Serruys PW, Onuma Y, Garcia-Garcia HM, et al. Dynamics of vessel wall changes following the implantation of the absorb everolimus-eluting bioresorbable vascular scaffold: a multi-imaging modality study at 6, 12, 24 and 36 months. EuroIntervention 2014;9:1271–84.

16. von Birgelen C, Klinkhart W, Mintz GS, et al. Plaque distribution and vascular remodeling of ruptured and nonruptured coronary plaques in the same vessel: an intravascular ultrasound study in vivo. J Am Coll Cardiol 2001;37:1864–70.

17. Virmani R, Burke AP, Farb A, Kolodgie FD. Pathology of the vulnerable plaque. J Am Coll Cardiol 2006;47 Suppl:C13–8.

18. Wentzel JJ, Schuurbiers JC, Gonzalo Lopez N, et al. In vivo assessment of the relationship between shear stress and necrotic core in early and advanced coronary artery disease. EuroIntervention 2013;9:989–95.

19. Kubo T, Maehara A, Mintz GS, et al. The dynamic nature of coronary artery lesion morphology assessed by serial virtual histology intravascular ultrasound tissue characterization. J Am Coll Cardiol 2010;55:1590–7.

20. Ruzsa Z, van der Linden M, Van Mieghem NM, et al. Culotte stenting with bioabsorbable everolimus-eluting stents. Int J Cardiol 2013;168:e35–7.

21. van Mieghem NM, Wilschut J, Ligthart J, Witberg K, van Geuns RJ, Regar E. Modified T-technique with bioresorbable scaffolds ensures complete carina coverage: an optical coherence tomography study. J Am Coll Cardiol Intv 2014;7:e109–10.

22. Karanasos A, van Geuns RJ, Zijlstra F, Regar E. Very late bioresorbable scaffold thrombosis after discontinuation of dual antiplatelet therapy. Eur Heart J 2014;35:1781.

23. Diletti R, Karanasos A, Muramatsu T, et al. Everolimus-eluting bioresorbable vascular scaffolds for treatment of patients presenting with ST-segment elevation myocardial infarction: BVS STEMI first study. Eur Heart J 2014;35:777–86.

24. Manfrini O, Mont E, Leone O, et al. Sources of error and interpretation of plaque morphology by optical coherence tomography [published correction appears in Am J Cardiol 2007;99:1350]. Am J Cardiol 2006;98:156–9.

25. Gonzalo N, Serruys PW, García-García HM, et al. Quantitative ex vivo and in vivo comparison of lumen dimensions measured by optical coherence tomography and intravascular ultrasound in human coronary arteries. Rev Esp Cardiol 2009;62:615–24.

KEY WORDS percutaneous coronary intervention, plaque, stents

APPENDIX For supplemental material, please see the online version of this article.